BOLETIN DE LA SOCIEDAD ESPAÑOLA DE
Cerámica y Vidrio
www.elsevier.es/bsecv

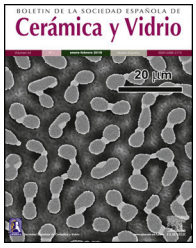

Original

Cured alkali-activated heated clay-cellulose composites: Microstructure, effect of glass addition and performances

Abdellah Mourak, Mohamed Hajjaji, Abdelhakim Alagui*

Laboratoire de Physico-chimie des Matériaux et Environnement, Faculté des Sciences Semlalia, Université Cadi Ayyad, B.P. 2390, Av. Pce My Abdellah, 40001 Marrakech, Morocco

ARTICLE INFO

Article history:
Received 28 May 2019
Accepted 15 January 2020
Available online 7 February 2020

Keywords:
Geopolymer
Heated clay
Cellulose
Alkaline activation
Microstructure
Performances

ABSTRACT

The co-presence of geopolymers and cellulose in clay-based materials could improve their performances. Thus, cured NaOH-activated heated clay-cellulose (up to 10 mass%) composites were prepared, and their microstructural characteristics were investigated. Moreover, the effect of waste glass addition on the composites characteristics was evaluated. The results showed that zeolite (chabazite) and sodium carbonate were formed from metakaolin and by carbonation respectively, and the zeolization process slowed down after 5 days of curing because of ions immobilization. The coating of metakaolin particles by the amorphous cellulose II-Na formed reduced drastically the formation of zeolite. The presence of cellulose II-Na resulted in the porosity decrease, and consequently the mechanical strength and density enhanced. The results also showed that the kinetics of water absorption by the composites followed the pseudo-first order equation, and the rate constant was found to be $4.3 \times 10^{-3}\ s^{-1}$. Moreover, the reinforcing effect of the cellulose fibbers was annihilated by the formation of glass derivatives.

Compuestos de arcilla-celulosa calentados activados por álcali: microestructura, efecto de la adición de vidrio y actuaciones

Palabras clave:
Geopolímeros
Arcilla calentada
Celulosa
Activación alcalina
Microestructura
Rendimiento

RESUMEN

La co-presencia de geopolímeros y celulosa en materiales a base de arcilla podría mejorar sus rendimientos. De este modo, se prepararon compuestos de arcilla-celulosa calentada activados con NaOH (hasta un 10% en masa) y se investigaron sus características microestructurales. Además, se evaluó el efecto de la adición de residuos de vidrio sobre las características de los composites. Los resultados mostraron que la zeolita (chabasita) y el carbonato de sodio se formaron a partir de metacaolín y por carbonación, respectivamente, y el proceso de zeolización se ralentizó después de 5 días de curado debido a la

* *Corresponding author.*
E-mail address: hajjaji@uca.ma (M. Hajjaji).
https://doi.org/10.1016/j.bsecv.2020.01.005

inmovilización de iones. El recubrimiento de partículas de metacaolín por la celulosa amorfa II-Na formada redujo drásticamente la formación de zeolita. La presencia de celulosa II-Na resultó en la disminución de la porosidad y, en consecuencia, la resistencia mecánica y la densidad aumentaron. Los resultados también mostraron que la cinética de la absorción de agua por los compuestos siguió la ecuación de pseudo primer orden, y se encontró que la constante de velocidad era $4{,}3 \times 10^{-3}\ s^{-1}$. Además, el efecto de refuerzo de las fibras de celulosa fue aniquilado por la formación de derivados de vidrio.

Introduction

Alkaline activation of aluminosilicates, such as dehydroxylated clay minerals, results in the formation of tri-dimensional polymeric structures (geopolymers) composed of attached tetrahedra units of silicate and aluminate denoted poly (silico-oxo-aluminate) [1–4]. Taking for instance the metakaolin ($Al_2O_3.2SiO_2$), the alkaline activation causes its dissolution, and consequently $Al(OH)_4^-$ and $[SiO_x(OH)_{4-x}]^{x-}/[Si_2O_{1+x}(OH)_{6-x}]^{x-}$ ions form [5]. These species can be combined together and give rise to oligomers, which in their turn lead to the formation of gels, then to the geopolymers. Referring to Yao et al. [6], the geopolymerisation process seemed to take place according to the following steps: destruction, polymerization and stabilization. In general, the geopolymerisation processes depend mainly on the alkali used and the chemical composition of the starting material, and on the curing conditions (temperature, time and atmosphere) [7–10]. Geopolymers are considered as eco-friendly cementitious materials [4,11–13].

Cellulose, which is a polysaccharide polymer, is the main structural constituent of plants. Because of its fibrous feature and remarkable ratio strength to density, cellulose is a convenient material for reinforcing cementing composites [14,15]. In addition to their good mechanical strength, cellulose-reinforced composites impede heat and sound transfer. The performance of cellulose fibbers in composites depends on their surface characteristics, dimensions and amounts. In this respect, it can be noted that in the contact of water, the cellulose-containing composites manifest low mechanical strength because of the high hydrophilic character of the cellulose fibbers [16]. To reduce this eventual negative impact, the surfaces of the cellulose fibbers are physically treated by using energetic radiations, such as UV and γ-radiations, or chemically modified by grafting [16]. The chemical modification of cellulose is also performed with concentrated NaOH solutions (18–32%) at 25–40 °C [17]. Under such conditions, the native form of cellulose (cellulose I) changes into cellulose II. Nevertheless, the cellulose stability depends on the alkaline conditions [18].

Referring to some authors, the suitable amounts of cellulose in cementing composites should be in the range of 0.2–2.0% v/v [15,19,20]. The use of high amounts of cellulose can yield appreciable absorption of water, and consequently the mechanical strength declines.

In highly alkaline solutions, glass is etched and various derivatives $(Si(OH)_4$, $(HO)_3Si\text{-}O\text{-}Si(OH)_3$, linear and cyclic trimmer, and polymer) form [21]. Referring to Torres-Carrasco and Puertas [22], waste glass seemed to be an effective alkaline activator in geopolymer preparation. Thereby, it was used as an ancillary activator in this study.

The co-presence of geopolymers and cellulose in clay-based composites can improve their performances because of the cementitious feature of geopolymers and the reinforcing effect of cellulose. So, in this work, the neoformation processes and the interactions between clay particles and fibres in cured NaOH-activated composites of a heated clay and cellulose were investigated, and their practical performances were evaluated. For this purpose, and based on the results published

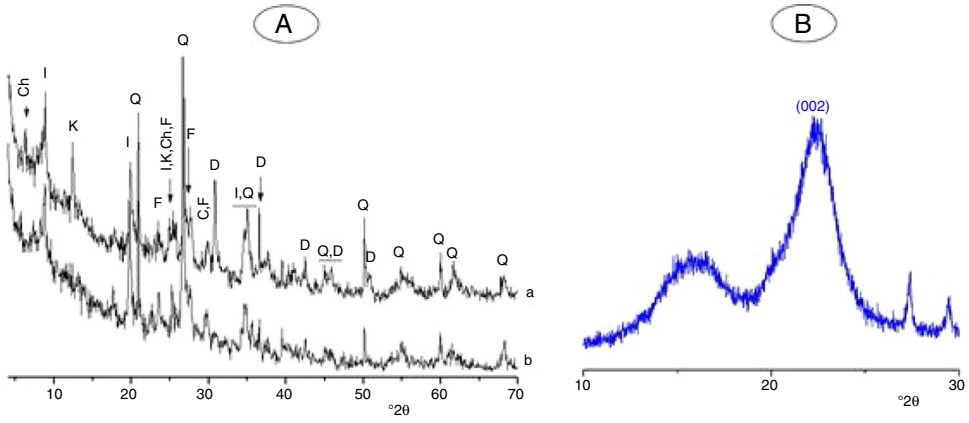

Fig. 1 – X-ray diffraction patterns of the clay (A) and the cellulose (B) used. (a) Raw clay; (b) clay heated at 700 °C for 2 h. Ch: chlorite; I: illite; K: kaolinite; Q: quartz; F: K-feldspar; C: calcite; D: dolomite.

Table 1 – Chemical compositions of the clay and the glass waste used, and the clay mineralogical composition.

	Chemical composition								
	SiO_2	Al_2O_3	Fe_2O_3	K_2O	MgO	CaO	Na_2O	TiO_2	*LOI
Clay	51.4	21.7	4.0	3.5	3.3	3.1	1.0	0.6	10.7
Waste glass	68.7	1.4	0.1	0.4	3.7	4.4	20.9	–	0.2

Clay mineralogical composition						
Illite	Kaolinite	Chlorite	Quartz	Dolomite	Hematite	K-feldspar
33	25	10	19	6	4	3

* Loss on ignition.

by El Hafid and Hajjaji [10], briquettes of cured NaOH-activated mixtures of heated clay and cellulose were prepared, and their microstructures were investigated. Moreover, their mechanical strength and physical properties (density, porosity and water absorption) were measured. Furthermore, the effects of waste glass addition on phase formation and mechanical/physical properties of the cellulose-rich mixture were investigated.

Materials, experimental procedures and techniques

Materials

Clay

The clay used was from an open pit of clay near the city of Safi (Morocco). It was composed of illite, kaolinite and chlorite, and non-clay minerals (Fig. 1A). The chemical and mineralogical compositions of the clay, determined following the method of Holtzapffel [23], and by X-ray fluorescence spectrometry respectively, are given in Table 1.

The clay was ground to pass through a 100 μm–sieve, and heated at 700 °C for 2 h. The heating resulted in the decomposition of kaolinite and chlorite (Fig. 1A, Fig. 2A), and the formation of metakaolin, which is identified by the FT-IR band at 560 cm^{-1} (Fig. 2A).

Cellulose fibbers

Cellulose fibbers were extracted from rachises of date palms (Phoenix dactylifera) located at the neighbourhood of the city of Marrakech (Morocco). The rachises were finely ground, and chemically treated by using a conventional Soxhlet extractor, and azeotropic mixture of ethanol and toluene. By doing so, the pigments and lipids were removed. The residue obtained was introduced in a solution of sodium hydroxide (2%), and kept for 2 h at 80 °C in order to get rid of hemicelluloses and lignin. Finally, the fibbers isolated were bleached with a solution of sodium chlorite (1.7%, w/v) at 70 °C. Details related to the experimental steps followed are given elsewhere [24,25].

Typical X-ray diffraction pattern and FT-IR spectrum of the cellulose prepared are shown in Figs. 1B and 2B. The

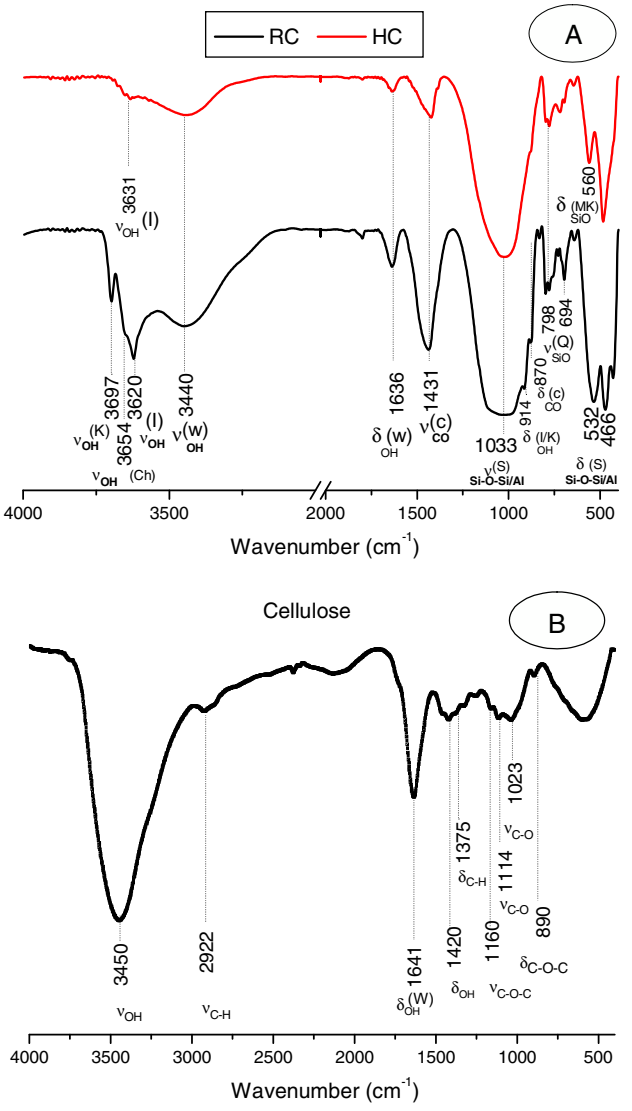

Fig. 2 – FT-IR spectra of the raw (RC) and heated (HC) clay (A), and the cellulose (B) used. K: kaolinite; Ch: chlorite; I: illite; W: water; C: carbonates; S: silicates; Q: quartz; MK: metakaolin.

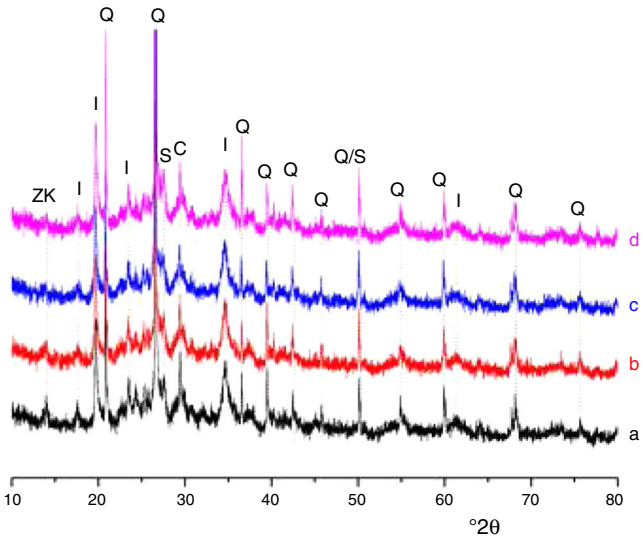

Fig. 3 – X-ray diffraction patterns of cured alkali-activated samples of cellulose and heated clay. (a) 0, (b) 2.5, (c) 5 and (d) 10 mass% cellulose. I: illite (PDF# 43-0685); Q: quartz (PDF# 05-0490); ZK: zeolite ZK (PDF#84-0698); C: calcite (PDF# 01-0837); S: sodium carbonate (PDF# 86-0298).

crystallinity index of the cellulose, determined according the method of Segal [26], was of 80%. The molecular weight of the cellulose measured following the method adopted by Ouajai and Shanks [27] and Thygesen et al. [28] was found to be 144,622 g/mol.

Glass

The waste glass, which was used as a supplementary source of silica for geopolymer formation, was a common soda-lime glass (Table 1). It was composed of 69% formers, 29% modifiers and 1% intermediates [29]. The glass was milled for 5 min with a PM100 Retsch planetary ball mill operating at 500 rpm. The 40 μm-sieved fraction, which corresponded to the grain size distribution D90, was dissolved in NaOH solution (6 M) under the following experimental conditions: operating time = 24 h, ambient temperature = 25 °C, stirring rate = 400 rpm.

Experimental procedures and techniques

Preparation of cured alkali-activated composites

Portions of dried cellulose (up to 10 mass%) and the heated clay were intimately mixed, and etched with a solution of NaOH (6 M). The weight ratio clay/water was of 2.5. Considering that the concentration of NaOH (24%) used lies within the range of 18–32%, the cellulose is supposed to be the object of transformation instead of degradation [17].

For glass-containing composite preparation, the waste glass solution mentioned above was added to a mixture of dried cellulose and heated clay. The dough obtained consisted of 10 mass% cellulose, 22 mass% glass, and 68 mass% heated clay. The cellulose amount was fixed based on the results presented below.

The above damped blends were homogenized by kneading for 15 min, and subjected to extrusion. The extruded briquettes (3.8 mm × 9.2 mm × 40 mm) were cured under the following conditions: curing temperature = 83 °C, curing time = 30 days, atmosphere = air. These curing conditions were adopted on the basis of the results of El Hafid and Hajjaji [10].

Characterization techniques

The X-ray diffraction (XRD) analysis was carried out on powder samples by using a Philips X'Pert MPD diffractometer equipped with a copper anode ($\lambda_{K\alpha}$ = 1.5418 Å). The Fourier-transform infrared (FT-IR) spectra were recorded in the range of 4000–400 cm^{-1} with a Perkin-Elmer Fourier-Transform 1720-x spectrophotometer. The samples analyzed were shaped as thin discs composed of 1 mg of material and 99 mg of KBr. The deconvolution of infrared bands and the determination of the bands areas were realized with the PeakFit v4.12 software (Peak type: Gaussian shape). The curves fit was evaluated on the basis of the values of *F*-statistic, standard error (SE)

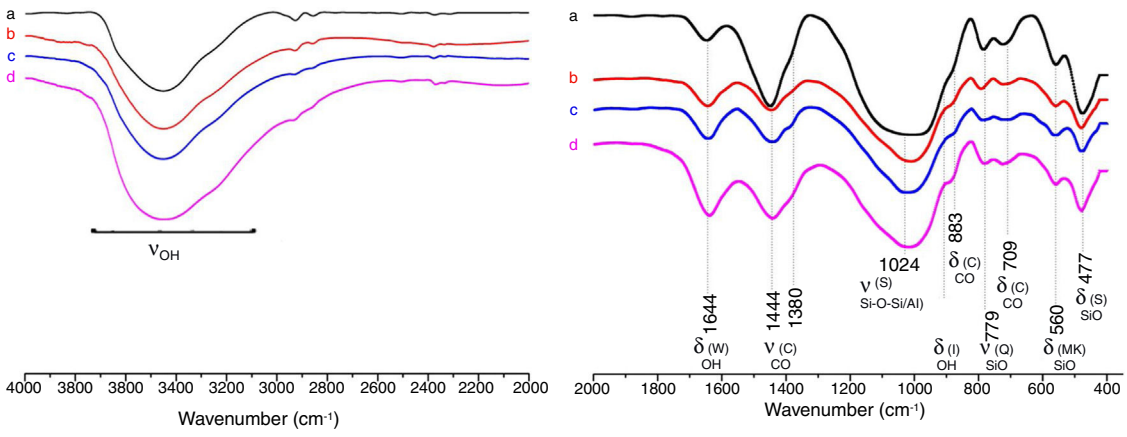

Fig. 4 – FT-IR spectra of the cured samples studied. The broad band in the range of 3700–3000 cm^{-1} is composed of bands related to the stretching vibrations of OH of illite/cellulose, physisorbed water, and constitutional waters of zeolite and gel. The bands attribution was done on the basis of the study of El Hafid and Hajjaji [29]. (a) 0, (b) 2.5, (c) 5 and (d) 10 mass% cellulose. W: water; C: carbonates; S: silicates; I: illite; Q: quartz; MK: metakaolin.

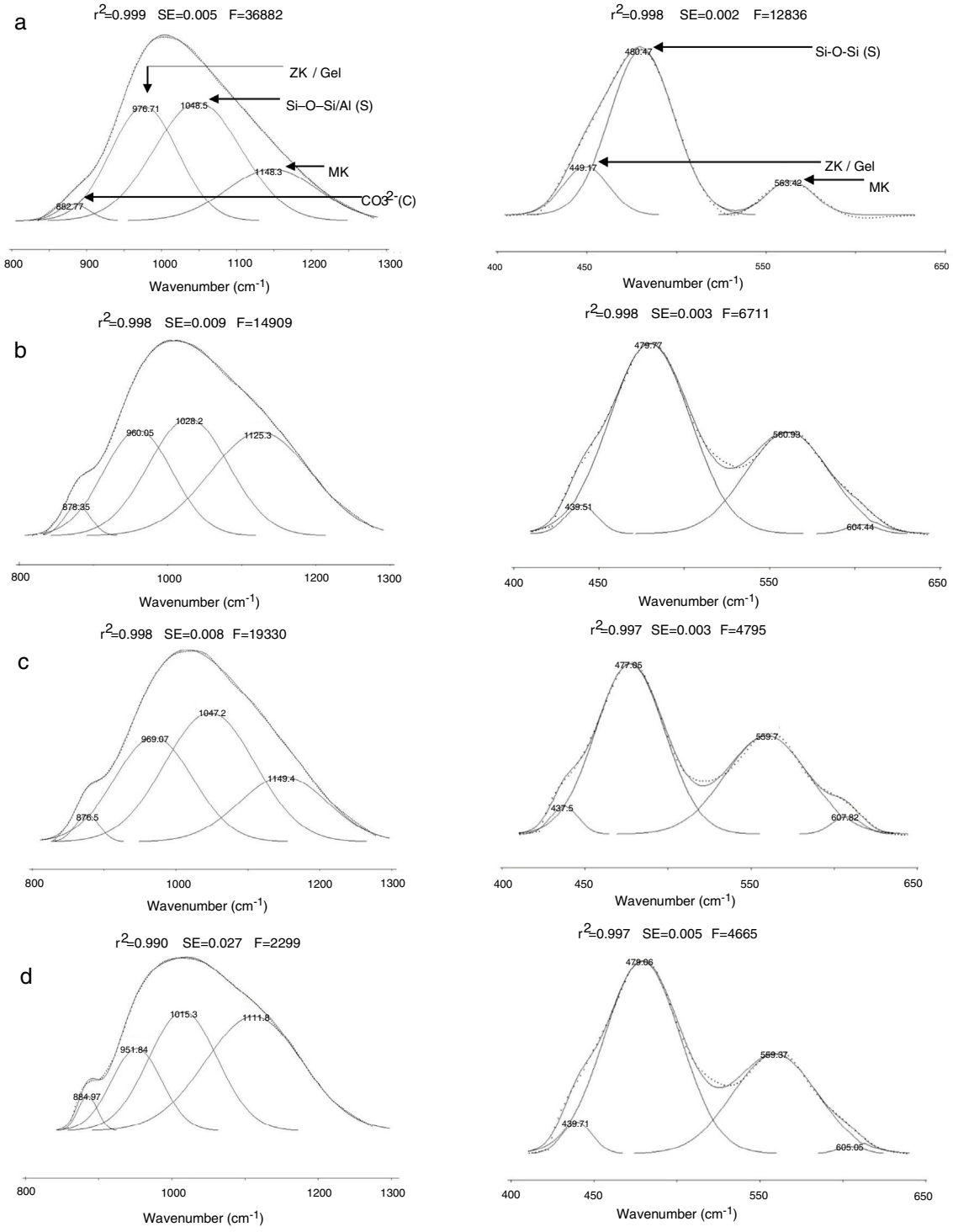

Fig. 5 – Deconvoluted FT-IR bands located at the finger print region. (a) 0, (b) 2.5, (c) 5 and (d) 10 mass% cellulose. ZK: zeolite; S: silicates; MK: metakaolin; C: carbonates. The bands were attributed on the basis of the work of El Hafid and Hajjaji [29].

and correlation coefficient (r^2) [30]. The best fitting curve corresponded to the highest values of F and r^2, and the lowest value of SE.

Microscopic examinations of the microstructure were performed on freshly fractured pieces of the cured samples with a Zeiss SupraVP40 scanning electron microscope (SEM), equipped with a 20 mm^2 X-Max diffusion silicon detector. For this purpose, the pieces were coated with a thin layer of carbon.

The flexural and compressive loads at failure were measured with an EX 150 DeltaLab apparatus, and the strengths were calculated according to the equations:

$$\sigma_{FS} = \frac{3F \cdot L}{2bh^2}$$

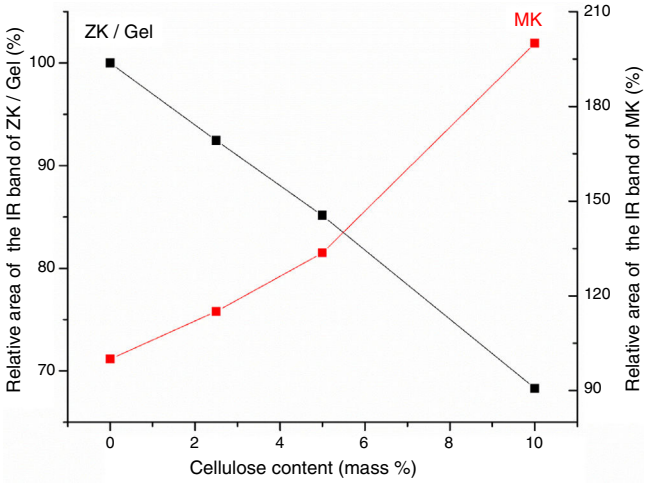

Fig. 6 – Variations of the relative areas of the IR bands associated to zeolite/gel (ZK/gel) and metakaolin (MK) against cellulose content.

$$\sigma_{CS} = \frac{F}{S}$$

(σ_{FS} and σ_{CS} are the flexural and compressive strengths respectively, F: load at failure; L: distance between the two supports (2.8 cm) of the apparatus; b and h are the width and the thickness of the test-bar). The measurements were performed in triplicate, and the standard deviations were in the range of 0.1–0.7 MPa.

The total porosity (P_T) of the cured briquettes was evaluated by using the equation:

$$P_T = 100\left(1 - \frac{\rho_a}{\rho_t}\right)$$

(ρ_a and ρ_t are the apparent and true densities. ρ_a was measured by pycnometry, using prismatic samples and edible oil as a solvent [31]. For the determination of ρ_t, the measurements were carried out on powder samples).

The electrical conductivity, which represents here the ability of aqueous dispersions of the composites studied to allow the ions transport by applying an alternating electrical current, was measured at room temperature by means of a TDS Metre con 510 conductimeter. The measurements were conducted on dispersions composed of 10 mL of distilled water and 1 g of the material studied.

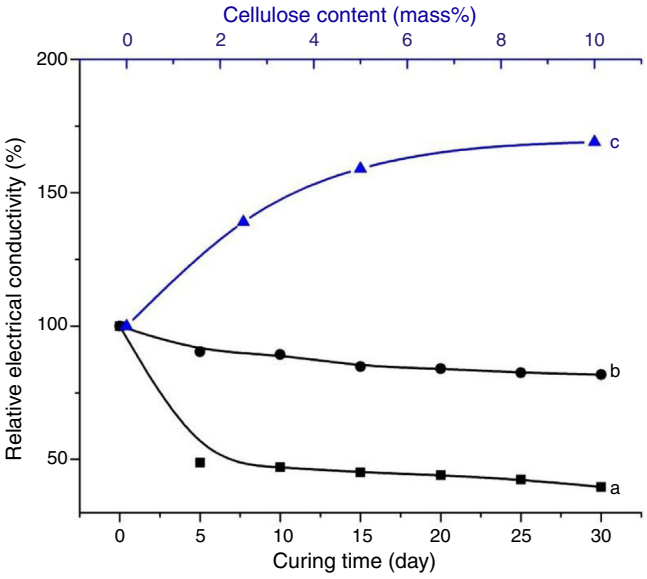

Fig. 8 – Variations of the relative electrical conductivity against curing time (a, b) and cellulose content (c). a: 0 mass% cellulose; b: 10 mass% cellulose.

The instantaneous amounts of water absorbed by the briquettes at room temperature were measured by weighting samples before and after contact with water. For this purpose, a water-submerged sponge was used as a source of water [31]. The maximum amount retained was determined after 5 min of contact, which was the equilibrium time.

Results and discussion

Microstructure characterization

As can be deduced from the typical XRD patterns shown in Fig. 3, the cured alkali-activated composites studied consisted of zeolite (chabazite) and sodium carbonate as neoformed phases. The carbonation of the composites occurred during the curing operation as a result of the reaction of the atmospheric CO_2 and Na^+ released by NaOH [10]. The intensity of the X-ray reflexion of zeolite ($^\circ 2\theta = 14$) declined with increasing the amount of cellulose, and the zeolite amount in the cellulose-rich composite seemed to be in the threshold of detection. In addition to the crystalline phases identified,

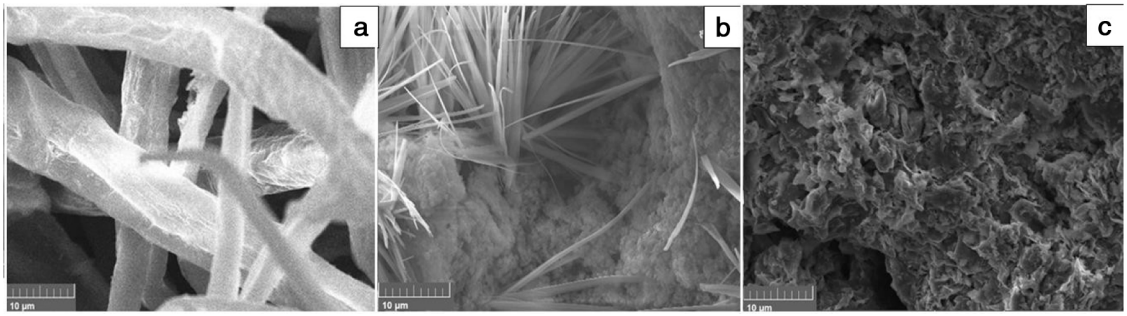

Fig. 7 – SEM micrographs of the cellulose fibres (a), zeolite particles formed in the cured heated clay (b), and the composite containing 10 mass% cellulose (c).

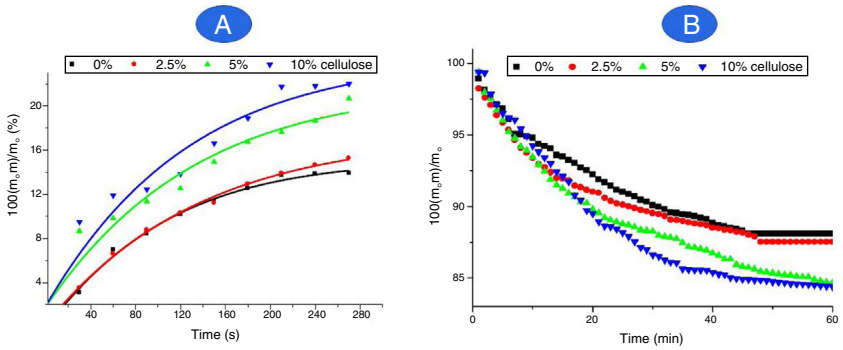

Fig. 9 – Evolution of the amounts of water retained (A) and released (B) by the composites studied as a function of time. m_o and m are the sample masses before and after experiments.

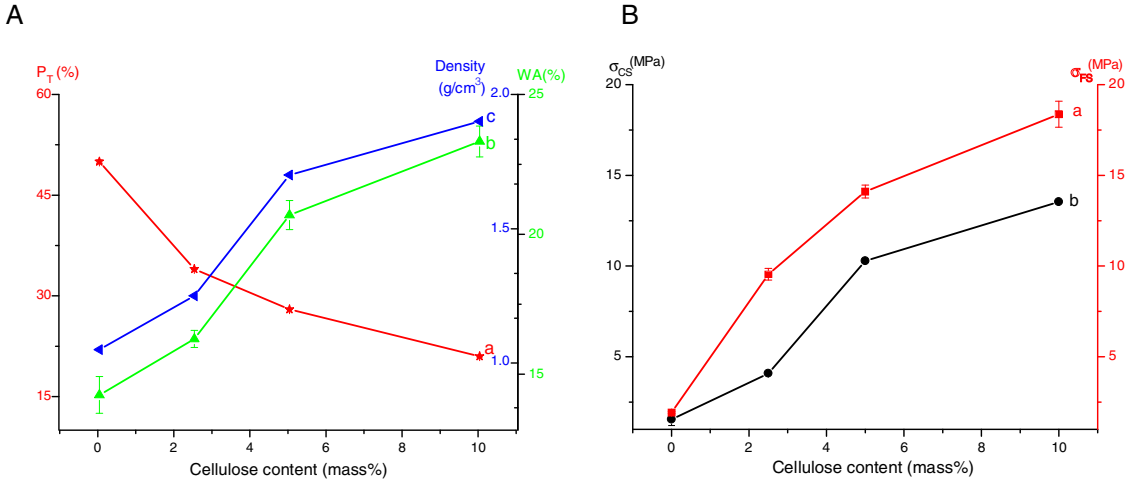

Fig. 10 – Changes of the physical (A) and mechanical (B) properties of the cured composites studied as a function of cellulose addition. (A): porosity (a), water absorption (b) and density (d). (B): flexural (a) and compressive (b) strengths.

the cured samples comprised metakaolinite, characterized by the FT-IR band at 560 cm^{-1} (Fig. 4). The characteristics bands of the main reaction products (gel and zeolite) did not manifest on the spectra given in Fig. 4 because of bands overlapping. The deconvolution of the FT-IR bands located at the finger print region revealed bands assignable to zeolite and gel (Fig. 5). Based on the areas of the bands of zeolite/gel (972 cm^{-1}) and metakaolin (560 cm^{-1}), the quantity of zeolite/gel regressed with increasing the cellulose amount, whereas that of metakaolin increased (Fig. 6). So, quantitative additions of cellulose impeded the reactivity of metakaolin, which is considered as the reactant for the zeolite formation [29].

Microscopic examinations of the cured materials showed that the original feature of fibbers of cellulose disappeared (Fig. 7). Moreover, the needle-like particles of zeolite, which were extensively formed in cured heated clay samples, vanished (Fig. 7).

Considering the evolutions of the electrical conductivity versus curing time shown in Fig. 8, the immobilization of ions, chiefly NaOH-derivatives ions, in cured cellulose-free samples took place after 5 days of ageing. In contrast, it occurred in early moments of etching of cellulose-containing heated clay. Furthermore, the mobility of the ions in the presence of cellulose was relatively high. This result suggested that cellulose was involved in the retention of OH^- and Na^+, but these ions were loosely attached. In addition, the reactions of zeolization and carbonation, which occurred in cellulose-free sample, reached their limits after 5 days of ageing. Referring to the change of the electrical conductivity against the cellulose content (Fig. 8), the ions mobility increased with increasing the cellulose amount. In conformity with the above result, ions of dissolved sodium hydroxide were mainly associated to cellulose fibbers, but they kept some mobility by application of an electrical field. In the presence of substantial amount of cellulose, e.g. 10 mass%, almost the entire OH^- ions were retained by cellulose. Therefore, the etching of metakaolin became limited, and consequently zeolite could not form.

In line with the reported studies, which dealt with NaOH-etched cellulose fibbers [32–36], it was believed that Na^+ ions adsorbed on cellulose fibbers, and consequently hydrogen bonds between chains of cellulose were broken. In such a condition, the conformations of chains changed, and cellulose II-Na formed. Likely because of the new configurations

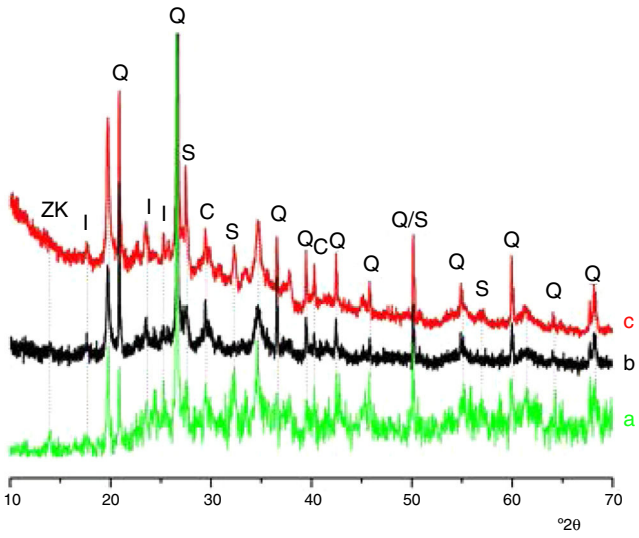

Fig. 11 – X-ray diffractograms of cured alkali-activated mixtures. (a): 22% glass-heated clay; (b): 10% cellulose-heated clay; (c): 10% cellulose-22% glass-heated clay. I: illite, S: sodium carbonate, ZK: zeolite ZK, Q: quartz, C: calcite.

of the chains, the fibrous aspect of cellulose disappeared. In this respect, it should be noted that the XRD analysis of the cured composites (Fig. 3) did not show any reflexion associated to cellulose II-Na because of its disorganized structure. Based on the above results, it was assumed that the chains of cellulose II-Na were attached to silanol groups, especially those of metakaolin, by means of hydrogen bonds and/or Van der Waals attractive interaction. The fixation of OH^- and Na^+ ions by cellulose II-Na, and the intense coating of metakaolin particles with cellulose fibbers were responsible for zeolite vanishing.

Retention and release of water

As can be deduced from Fig. 9A, more than 85 mass% of water retained by the composites was absorbed in less than 3.5 min of contact, and saturation was reached nearby 5 min. The variation of the retained amount versus time (up to 3.5 min) obeyed the pseudo-first order kinetics relation:

$$Ln\frac{\Delta m}{m_o} = -kt + A \quad (1)$$

(Δm: the weight of water retained; m_o: mass of the dried sample used; k is considered as a rate constant; A is a constant).

The rate constant was independent of the amount of cellulose, and its value was found to be $4.3 \times 10^{-3}\ s^{-1}$. Thus, the transport of water was not influenced by the cellulose content.

Referring to Fig. 9A, cellulose addition resulted in an increase in water absorption (WA), and the relation followed was:

$$WA = 0.94\,\tau + 14.53 \quad (2)$$

(τ is the cellulose content). Thus, water absorption by the cured samples was chiefly linked to the presence of cellulose, known as a hydrophilic material.

Taking into consideration Fig. 9B, the water retained by the composites was gradually eliminated in less than 30 min. The application of the above kinetics equation allowed to differentiate three stages: Up to about 8 min, the rate of water released (k_r) increased from $5.3 \times 10^{-3}\ min^{-1}$ to $9.4 \times 10^{-3}\ min^{-1}$ as the cellulose amount rose from 2.5 to 10 mass%. In the intermediate stage ($8 < t < 20$ min), k_r varied in the range of $(2.0–5.3) \times 10^{-3}\ min^{-1}$, and in the final span 25–30 min, k_r evolved from $1.3 \times 10^{-3}\ min^{-1}$ to $3.3 \times 10^{-3}\ min^{-1}$. Thus, it was believed that in the first stage, only weakly attached molecules, such as those retained by Van der Waals forces

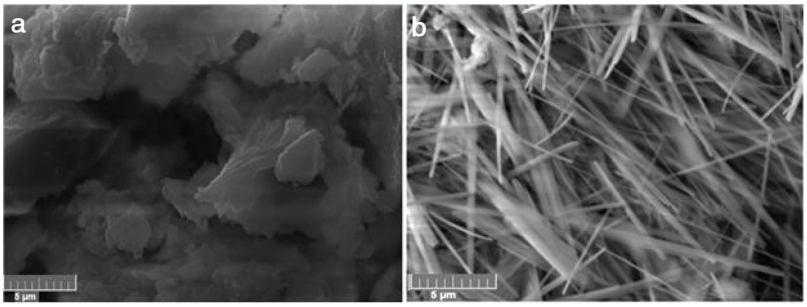

Fig. 12 – SEM micrographs showing the microstructure of the cured mixture 10% cellulose-22% glass-heated clay (a), and interlocking needle-like zeolite formed in the cured glass-heated clay binary (b).

Table 2 – Bending strength and water absorption of cured alkali-activated composites.

Cured alkali-activated composites	Bending strength (MPa)		Water absorption (%)	
	Mean value	SD	Mean value	SD
10% cellulose -22% glass - heated clay	6.8		23	
10% cellulose-heated clay	18.0	0.1–0.2	23	0.3–0.7
22% glass-heated clay	6.5		20	

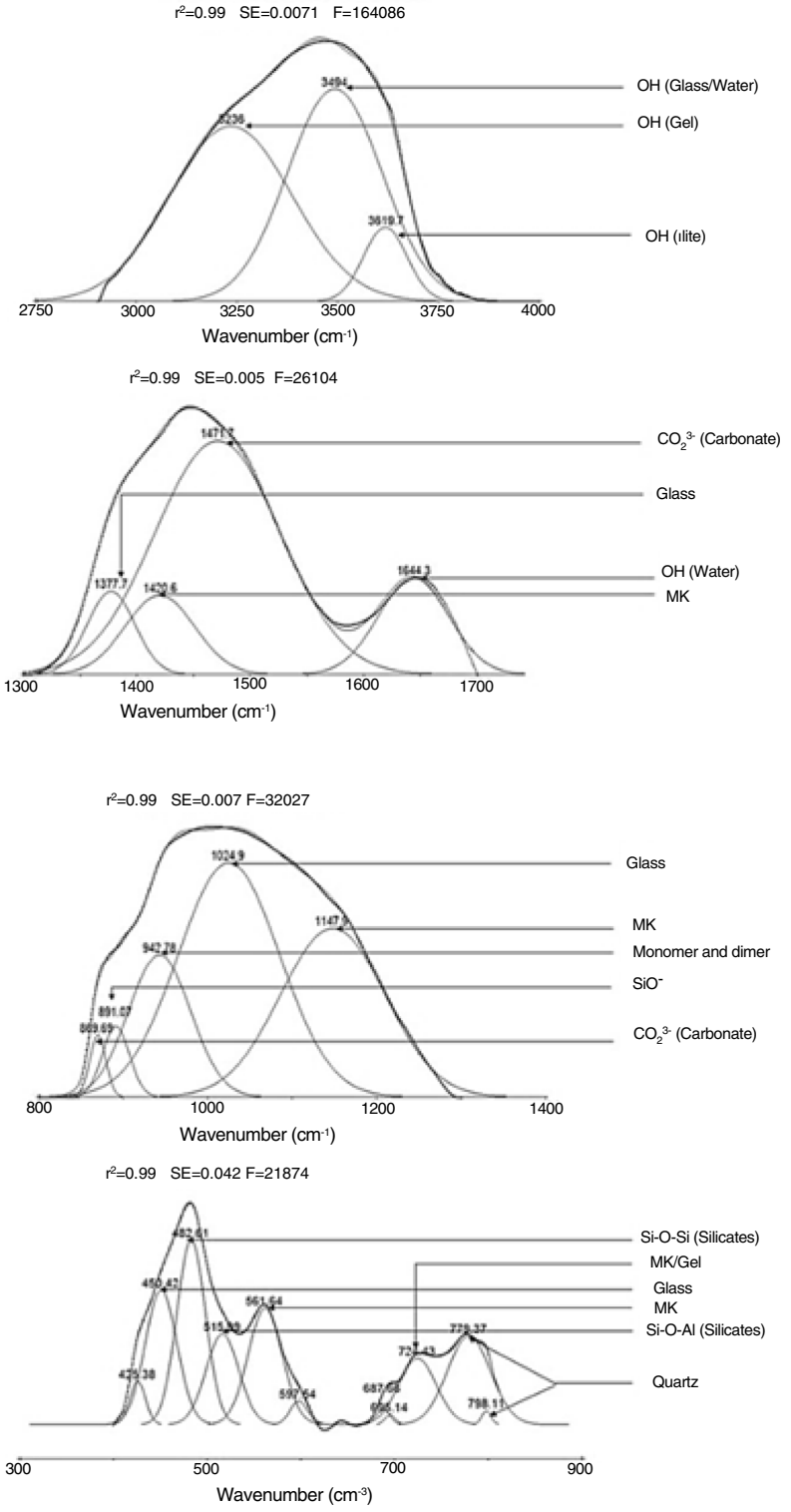

Fig. 13 – Deconvoluted bands in the IR spectrum of the ternary system studied. The assignment of the bands was done on the basis of the study of El Hafid and Hajjaji [29].

were released. The water molecules, which developed mild to strong attractive electrostatic interactions, mainly with cellulose fibbers, were released during the intermediate and final stages. The attractions involved in the final stage were probably accomplished by hydrogen bonds.

Mechanical strength

The flexural strength as well as the compressive strength of the cured composites enhanced with increasing cellulose amount (Fig. 10B). The strengthening of the composites

was accompanied by a reduction of porosity and an increase of density (Fig. 10A). Thus, cellulose II amorphous phase favoured the compaction process, and consequently strengths enhanced. Considering the changes of P_T and σ_{FS} against cellulose content (Fig. 10), the flexural strength and porosity were related according to the equation:

$$\sigma_{FS}\,(\text{MPa}) = -56.63P_T + 29.82 \quad (3)$$

It is worth noting that up to 10 mass% cellulose, water retention did not alter the mechanical strength of the composites.

In comparison to some geopolymer composites reinforced with natural fibres [37], the composites studied showed good bending strength, and moderate compressive resistance.

Glass-containing mixture

Based on the XRD pattern given in Fig. 11, the cured glass-containing mixture was composed of original minerals (illite, calcite and quartz), and sodium carbonate (neoformed phase). Zeolite, which was formed in cellulose-lean mixtures as well as in cured glass-heated clay binary (Fig. 11) was not detected, probably because its amount is below the detection threshold. In this respect, it could be recalled that the XRD analysis of the cellulose-rich briquette did not show the presence of the main X-ray reflection of zeolite (Fig. 11).

The microstructure of this cured ternary mixture consisted of widespread coated particles such as shown in Fig. 12a. The acicular particles of zeolite, which were extensively encountered in cured glass-heated clay (Fig. 12b), were not observed. Thus, the presence of glass did not impede clay particles wrapping by cellulose II-Na fibbers. Due to the glass dissolution, the amount of free sodium rose, and consequently the quantity of sodium carbonate increased.

Glass addition to the cellulose-heated clay binary resulted in the decline of the mechanical strength, but its influence on water absorption was not significant (Table 2). The strength and water absorption of glass-containing mixture were very close to those of the cured binary system glass-heated clay (Table 2). Thus, it was believed that due to the formation of the glass-derivatives species identified in Fig. 13, the conformations of the chains of cellulose II-Na were affected, and consequently their reinforcing effect was annihilated.

Conclusion

The results of this study yielded the following conclusions: (i) Zeolite (chabazite) and sodium carbonate formed in cured alkali-activated heated clay-cellulose composites. The zeolite formation became limited as the cellulose amount reached 10 mass%, and also after 5 days of ageing. These facts were due to the metakaolin particles coating by the cellulose II-Na fibbers, and to the immobilization of NaOH derivatives respectively. (ii) Because of the abundance of cellulose II-Na, the bending strength and water absorption of the composites evolved from 1.7 to 17.4 MPa, and from 11.3 to 19% respectively. These facts were linked to the reduction of porosity due essentially to the compaction intensification. (iii) Water retention as well as water release by the composites versus time followed the pseudo-first order kinetic equation. The kinetics of water absorption was a mono-stage process. In contrast, different stages were distinguished for water release. These were taken as an indication of the involvement of different electrostatic forces between water molecules and geopolymer particles. (iv) The presence of glass in the cured cellulose-heated clay binary did not affect the nature of crystalline phases formed, but it annihilated the reinforcing effect of cellulose fibbers. The latter fact was chiefly associated to the alteration of the conformations of the chains of cellulose II-Na by the formation of various glass derivatives.

Acknowledgement

The authors are grateful to CNRST (Morocco) for its financial support (grant no. PPR/26/2015).

REFERENCES

[1] J. Davidovits, Geopolymers: inorganic polymeric new materials, J. Therm. Anal. 37 (1991) 1633–1656, http://dx.doi.org/10.1007/BF01912193.
[2] P. Duxson, A. Fernández-Jiménez, J.L. Provis, G.C. Lukey, A. Palomo, J.S.J. Van Deventer, Geopolymer technology: the current state of the art, J. Mater. Sci. 42 (2007) 2917–2933, http://dx.doi.org/10.1007/s10853-006-0637-z.
[3] J.L. Provis, J.S.J. Van Deventer, Geopolymers: Structure, Processing, Properties and Industrial Applications, CRC Press, Woodhead Publishing Limited, 2009.
[4] L.K. Turner, F.G. Collins, Carbon dioxide equivalent (CO_2-e) emissions: a comparison between geopolymer and OPC cement concrete, Constr. Build. Mater. 43 (2013) 125–130, http://dx.doi.org/10.1016/j.conbuildmat.2013.01.023.
[5] C. Li, H. Sun, L. Li, A review: the comparison between alkali-activated slag (Si + Ca) and metakaolin (Si + Al) cements, Cem. Concr. Res. 40 (2010) 1341–1349, http://dx.doi.org/10.1016/j.cemconres.2010.03.020.
[6] X. Yao, Z. Zhang, H. Zhu, Y. Chen, Geopolymerization process of alkali–metakaolinite characterized by isothermal calorimetry, Thermochim. Acta 493 (2009) 49–54, http://dx.doi.org/10.1016/j.tca.2009.04.002.
[7] F. Pacheco-Torgal, J. Castro-Gomes, S. Jalali, Alkali-activated binders: a review. Part 2. About materials and binders manufacture, Constr. Build. Mater. 22 (2008) 1315–1322, http://dx.doi.org/10.1016/j.conbuildmat.2007.03.019.
[8] P. Rovnaník, Effect of curing temperature on the development of hard structure of metakaolin-based geopolymer, Constr. Build. Mater. 24 (2010) 1176–1183, http://dx.doi.org/10.1016/j.conbuildmat.2009.12.023.
[9] A.D. Hounsi, G.L. Lecomte-Nana, G. Djétéli, P. Blanchart, Kaolin-based geopolymers: effect of mechanical activation and curing process, Constr. Build. Mater. 42 (2013) 105–113, http://dx.doi.org/10.1016/j.conbuildmat.2012.12.069.
[10] K. El Hafid, M. Hajjaji, Effects of the experimental factors on the microstructure and the properties of cured alkali-activated heated clay, Appl. Clay Sci. 116–117 (2015) 202–210, http://dx.doi.org/10.1016/j.clay.2015.03.015.
[11] B.C. McLellan, R.P. Williams, J. Lay, A. Van Riessen, G.D. Corder, Costs and carbon emissions for geopolymer pastes in comparison to ordinary portland cement, J. Clean. Prod. 19 (2011) 1080–1090, http://dx.doi.org/10.1016/j.jclepro.2011.02.010.

[12] J.S.J. Van Deventer, J.L. Provis, P. Duxson, Technical and commercial progress in the adoption of geopolymer cement, Miner. Eng. 29 (2012) 89–104, http://dx.doi.org/10.1016/j.mineng.2011.09.009.
[13] A.M. Rashad, Metakaolin as cementitious material: history, scours, production and composition – a comprehensive overview, Constr. Build. Mater. 41 (2013) 303–318, http://dx.doi.org/10.1016/j.conbuildmat.2012.12.001.
[14] N. Neithalath, J. Weiss, J. Olek, Acoustic performance and damping behavior of cellulose-cement composites, Cem. Concr. Compos. 26 (2004) 359–370, http://dx.doi.org/10.1016/S0958-9465(03)00020-9.
[15] L. Yan, B. Kasal, L. Huang, A review of recent research on the use of cellulosic fibres, their fibre fabric reinforced cementitious, geo-polymer and polymer composites in civil engineering, Compos. Part B: Eng. 92 (2016) 94–132, http://dx.doi.org/10.1016/j.compositesb.2016.02.002.
[16] M.N. Belgacem, A. Gandini, The surface modification of cellulose fibres for use as reinforcing elements in composite materials, Compos. Interfaces 12 (2005) 41–75, http://dx.doi.org/10.1163/1568554053542188.
[17] T. Budtova, P. Navard, Cellulose in NaOH–water based solvents: a review, Cellulose, Springer Verlag 23 (1) (2016) 5–55, http://dx.doi.org/10.1007/s10570-015-0779-8.hal-01247093.
[18] C.J. Knill, J.F. Kennedy, Degradation of cellulose under alkaline conditions, Carbohydr. Polym. 51 (2003) 281–300.
[19] M. Ardanuy, J. Claramunt, R.D. Toledo Filho, Cellulosic fiber reinforced cement-based composites: a review of recent research, Constr. Build. Mater. 79 (2015) 115–128, http://dx.doi.org/10.1016/j.conbuildmat.2015.01.035.
[20] J. Wei, C. Meyer, Degradation mechanisms of natural fiber in the matrix of cement composites, Cem. Concr. Res. 73 (2015) 1–16, http://dx.doi.org/10.1016/j.cemconres.2015.02.019.
[21] P.W.J.G. Wijnen, T.P.M. Beelen, J.W. de Haan, C.P.J. Rummens, L.J.M. van de Ven, R.A. van Santen, Silica gel dissolution in aqueous alkali metal hydroxides studied by ^{29}Si-NMR, J. Non-Cryst. Solids 109 (1989) 85–94, http://dx.doi.org/10.1016/0022-3093(89)90446-8.
[22] M. Torres-Carrasco, F. Puertas, Waste glass in the geopolymer preparation. Mechanical and microstructural characterisation, J. Clean. Prod. 90 (2015) 397–408, http://dx.doi.org/10.1016/j.jclepro.2014.11.074.
[23] T. Holtzapfell, Les minéraux argileux, Société Géologique du Nord (SGN), Publication No. 12, Université de Lille (Villeneuve d'Ascq, France), 1985.
[24] F.W. Herrick, R.L. Casebier, J.K. Hamilton, K.R. Sandberg, Microfibrillated cellulose: morphology and accessibility, J. Appl. Polym. Sci.: Appl. Polym. Symp. 37 (1983) 797–813.
[25] A.F. Turbak, F.W. Snyder, K.R. Sandberg, Microfibrillated cellulose, a new cellulose product: properties, uses, and commercial potential, J. Appl. Polym. Sci.: Appl. Polym. Symp. 37 (1983) 815–827.
[26] L. Segal, J.J. Creely, A.E. Martin, C.M. Conrad, An empirical method for estimating the degree of crystallinity of native cellulose using the X-ray diffractometer, Text. Res. J. 29 (1959) 786–794, http://dx.doi.org/10.1177/004051755902901003.
[27] S. Ouajai, R.A. Shanks, Composition, structure and thermal degradation of hemp cellulose after chemical treatments, Polym. Degrad. Stabil. 89 (2005) 327–335, http://dx.doi.org/10.1016/j.polymdegradstab.2005.01.016.
[28] A. Thygesen, J. Oddershede, H. Lilholt, A.B. Thomsen, K. Ståhl, On the determination of crystallinity and cellulose content in plant fibres, Cellulose 12 (2005) 563–576, http://dx.doi.org/10.1007/s10570-005-9001-8.
[29] K. El Hafid, M. Hajjaji, Geopolymerization of glass- and silicate-containing heated clay, Constr. Build. Mater. 159 (2018) 598–609, http://dx.doi.org/10.1016/j.conbuildmat.2017.11.018.
[30] M. Wojdyr, Fityk: a general-purpose peak fitting program, J. Appl. Crystallogr. 43 (2010) 1126–1128, http://dx.doi.org/10.1107/S0021889810030499.
[31] K. El Hafid, M. Hajjaji, Alkali-etched heated clay: microstructure and physical/mechanical properties, J. Asian Ceram. Soc. 4 (2016) 234–242, http://dx.doi.org/10.1016/j.jascer.2016.07.001.
[32] T. Okanot, A. Sark, Intermediates and a possible mercerization mechanism, J. Appl. Polym. Sci. 30 (1985) 325–332, http://dx.doi.org/10.1002/app.1985.070300128.
[33] H. Nishimura, T. Okano, A. Sarko, Mercerization of cellulose. 5. Crystal and molecular structure of Na-cellulose I, Macromolecules 24 (1991) 759–770, http://dx.doi.org/10.1021/ma00003a020.
[34] Y. Nishiyama, S. Kuga, T. Okano, Mechanism of mercerization revealed by X-ray diffraction, J. Wood Sci. 46 (2000) 452–457, http://dx.doi.org/10.1007/BF00765803.
[35] E. Dinand, M. Vignon, H. Chanzy, L. Heux, Mercerization of primary wall cellulose and its implication for the conversion of cellulose I → cellulose II, Cellulose 9 (2002) 7–18, http://dx.doi.org/10.1023/A:1015877021688.
[36] I. Carrillo-Varela, M. Pereira, R.T. Mendonça, Determination of polymorphic changes in cellulose from Eucalyptus spp. fibres after alkalization, Cellulose 25 (2018) 6831–6845, http://dx.doi.org/10.1007/s10570-018-2060-4.
[37] K. Korniejenko, E. Frączek, E. Pytlak, M. Adamski, Mechanical properties of geopolymer composites reinforced with natural fibers, Proc. Eng. 151 (2016) 388–393, http://dx.doi.org/10.1016/j.proeng.2016.07.395.